Reference: *Biol. Bull.* **214:** 122–134. (April 2008)

Reciprocal Changes in Calcification of the Gastrolith and Cuticle During the Molt Cycle of the Red Claw Crayfish *Cherax quadricarinatus*

ASSAF SHECHTER[1,3], AMIR BERMAN[2,3,4], ALON SINGER[2,3], AVIAD FREIMAN[1,3], MOR GRINSTEIN[5], JONATHAN EREZ[4], ELIAHU D. AFLALO[1,3], AND AMIR SAGI[1,3,*]

[1]*Department of Life Sciences,* [2]*Department of Biotechnology Engineering,* [3]*National Institute for Biotechnology in the Negev (NIBN), and* [4]*Ilse Katz Center for Nanoscience and Nanotechnology and Reimund Stadler Minerva Center for Mesoscale Macromolecular Engineering, Ben-Gurion University of the Negev, P.O. Box 653, Beer-Sheva 84105, Israel; and* [5]*The Institute of Earth Sciences, The Hebrew University of Jerusalem, Jerusalem 91904, Israel*

Abstract. Mobilization of calcium during the molt cycle from the cuticle to transient calcium deposits is widely spread in crustaceans. The dynamics of calcium transport to transient calcium deposits called gastroliths and to the cuticle over the course of the molt cycle were studied in the crayfish *Cherax quadricarinatus*. In this species, calcium was deposited in the gastroliths during premolt and transported back to the cuticle during postmolt, shown by digital X-ray radiograph analysis. The predominant mineral in the crayfish is amorphous calcium carbonate embedded in an organic matrix composed mainly of chitin. Scanning electron micrographs of the cuticle during premolt showed that the endocuticle and parts of the exocuticle were the source of most of the labile calcium, while the epicuticle did not undergo degradation and remained mineralized throughout the molt cycle. The gastroliths are made of concentric layers of amorphous calcium carbonate intercalated between chitinous lamella. Measurements of pH and calcium levels during gastrolith deposition showed that calcium concentrations in the gastroliths, stomach, and muscle were about the same (10 to 11 mmol l^{-1}). On the other hand, pH varied greatly, from 8.7 $\pm$ 0.15 in the gastrolith cavity through 7.6 $\pm$ 0.2 in muscle to 6.9 $\pm$ 0.5 in the stomach.

Received 27 May 2007; accepted 31 October 2007.

*To whom correspondence should be addressed. E-mail: sagia@bgu.ac.il

Abbreviations: ACC, amorphous calcium carbonate; FTIR, Fourier transform infrared spectroscopy; MMI, molt mineralization index.

Introduction

In most crustaceans, the rigid exoskeleton—cuticle—contains much of the stored calcium (Wheatly and Ayers, 1995). Produced by the underlying epidermal cells, the cuticle is composed of four layers (from outer to inner): epicuticle, exocuticle, endocuticle, and membranous layer (Travis and Friberg, 1963b; Raz *et al.*, 2002). The exocuticle and endocuticle, which make up most of the cuticle, comprise calcified matrixes of chitin and proteins, with the chitin-protein fibers stacked in layers of continuously changing orientation (Giraudguille, 1984; Roer and Dillaman, 1984). The thin epicuticle, which is composed of protein, lipids, and calcium but no chitin, has a dense bilaminar organization, with a basal layer that is pervaded by mineral-filled canals normal to the surface. The membranous layer also contains chitin and proteins, but it is not calcified (Roer and Dillaman, 1984; Aiken and Waddy, 1992). The main mineral found in the calcified layers of the cuticle is calcium carbonate (Greenaway, 1985; Wheatly and Ayers, 1995; Luquet and Marin, 2004).

The growth process in crustaceans demands periodic shedding and replacement of the cuticle during ecdysis. In some crustaceans, molting and ecdysis can take place throughout the life cycle, whereas other species molt only until sexual maturity is reached (Hartnoll, 1982). The principal source of the calcium required for building the cuticle is seawater, the natural habitat of most crustacean species. Calcium concentration in seawater is about 10 mmol l^{-1} (Greenaway, 1985). In crustacean species living on land or

in fresh water, where calcium availability is low—as in the case of our model organism the freshwater red claw crayfish *Cherax quadricarinatus* (von Martens)—calcium is obtained by reabsorbing it from the cuticle prior to shedding and storing it in transient calcium deposits (McWhinnie, 1962; Travis, 1963b; Willig and Keller, 1973; Ueno, 1980).

In crayfish these deposits are a pair of disc-like structures known as gastroliths, located on both sides of the stomach wall (Travis, 1960, 1963a, b; Travis and Friberg, 1963a). Gastroliths are also found in other decapods such as lobsters and some land crabs (Luquet and Marin, 2004). Gastroliths are formed in a cavity between the columnar epithelium of the gastrolith disc and the cardiac stomach wall. The main functions of the epithelium are the transport of hemolymph calcium to the gastrolith and the synthesis of the gastrolith organic matrix (Ueno, 1980).

The crustacean molt cycle is made up of the following stages: premolt, molt (ecdysis), postmolt, and intermolt; the last is the longest stage (Drach and Tchernigovtzeff, 1967), during which most of the calcium is stored in the cuticle. As the animal approaches premolt, the exoskeleton undergoes partial degradation, with the calcium ions being dissolved out of the mineralized matrix and transferred through the integumentary epithelium to the hemolymph (Ahearn *et al.*, 2004). The calcium ions are taken up from the hemolymph to form the gastroliths. During ecdysis, the gastroliths collapse into the stomach, where they are digested. After ecdysis, rapid remineralization of the cuticle during the postmolt stage relies on the calcium digested from the gastroliths together with exogenous calcium absorbed from the surrounding water. This massive calcium accumulation is illustrated in reports of crustaceans that double their cuticle calcium content as early as 12 h after ecdysis (Greenaway, 1985). Calcium originating from the gastrolith provides an immediate endogenous source for the calcification of essential body parts such as mouthparts and walking legs (Willig and Keller, 1973; Aiken and Waddy, 1992; Wheatly and Ayers, 1995).

In many crustaceans this cyclic metabolism of calcium from the exoskeleton to the temporary storage deposits and back is made possible by calcium carbonate polymorphism. In most crustacean species, exoskeleton calcium carbonate exists in two polymorphs, mainly the stable crystalline form, calcite (Yano, 1975; Pratoomchat *et al.*, 2002; Luquet and Marin, 2004), and some of the less stable form, amorphous calcium carbonate (ACC) (Greenaway, 1985; Addadi *et al.*, 2003; Sugawara *et al.*, 2006). Early reports claimed that gastrolith calcium carbonate occurs either as calcite (Travis, 1963b; Ueno, 1980) or in a poorly crystalline state (Travis, 1963c). However, more recent studies suggest that ACC is the major form in most temporary calcium carbonate deposits, such as the gastroliths (Addadi *et al.*, 2003). The stabilization of the otherwise unstable amorphous form probably requires unique conditions and the mediation of specialized macromolecules. The means of stabilizing ACC in crustaceans have yet to be elucidated. Several mechanisms for Ca^{2+} and H^{+} transport across the epithelium of transient calcium deposits in crustaceans have been proposed (Ziegler *et al.*, 2005). Studies of corals suggest that the precipitation of calcium carbonate may be controlled by an upward shift in pH at the calcification site (Al-Horani *et al.*, 2003).

Since calcium accumulation in the gastroliths is intimately connected to the molt cycle, the size of the gastroliths may be used as a premolt indicator (Pavey and Fielder, 1990), complementing the classical molt-staging method of Drach and Tchernigovtzeff (1967). To follow these changes occurring in the gastroliths, a noninvasive X-ray radiography technique was applied in several studies (McWhinnie, 1962; Rao *et al.*, 1977; Nakatsuji *et al.*, 2000; Shechter *et al.*, 2007). That technique was applied in this study, together with Fourier transform infrared (FTIR) spectroscopy and scanning electron microscopy (SEM), to follow the dynamics of biomineralization through the molt cycle during calcification and decalcification of the two calcium carbonate deposition sites—the multi-layered cuticle and the gastrolith—of *C. quadricarinatus*.

Material and Methods

Animals

Cherax quadricarinatus males were grown in and collected from artificial ponds at Ben-Gurion University of the Negev, Beer-Sheva, Israel. Food comprising shrimp pellets (Rangen Inc., Buhl, ID, USA, 30% protein) and wheat grain was supplied *ad libitum* three times a week. Temperature was kept at 27 ± 2 °C, and a photoperiod of 14 h light and 10 h dark was applied. Water quality was assured by circulating the entire volume of water through a bio-filter. The pH of the water was 8.3 ± 0.5, the nitrite concentration was less than 0.1 mg l^{-1}, the nitrate concentration was less than 50 mg/l, ammonium levels were negligible, and oxygen levels exceeded 5 mg l^{-1}. Animals were anesthetized in ice-cold water prior to dissection.

Endocrine induction of the molt cycle

Endocrine induction of the molt cycle by removal of the X-organ–sinus gland (XO-SG) (Shechter *et al.*, 2005) was performed exclusively in intermolt male crayfish that had no apparent gastroliths when observed using digital X-ray imaging. The XO-SG complex was removed by bilateral excision of the eyestalk with a surgical blade. Following the surgery, crayfish were held in individual cages for up to 19 days.

X-ray imaging and molt staging

Changes in mineralization during the molt cycle were monitored daily by digital X-ray radiography (Instrument Imaging, Focus model). Radiography conditions (60 kV, exposure time 0.05 s) were calibrated to avoid overexposure or underexposure. Images were acquired with a digital sensor (Schick technologies) USB CDR size 2. The molt stages of each crayfish were determined in terms of gastrolith growth according to the molt mineralization index (MMI). For each animal, the MMI is defined as the ratio of the gastrolith width (as observed in the X-ray imaging) to the carapace length. To calculate the gastrolith width, a round metal disc with a diameter of 10 mm was used for size calibration. Crayfish were classified as follows: interolt—MMI of 0, signifying the complete absence of gastroliths; premolt—MMI of up to 0.14; postmolt—after ecdysis, apparent gastroliths in the stomach.

Digital X-ray radiographs analysis

Digital images were converted from 24-bit color into 8-bit, 256-greyscale format in MATLAB (The MathWorks, Inc.) and presented as three-dimensional maps in which X-ray opaque regions are brighter and higher and X-ray transparent regions are darker and lower. For each radiograph, the intensities of both the gastrolith and the cuticle that surrounds it were determined. The relative changes in mineral contents for each animal's organs were plotted as normalized intensity (I/I_{max}), where I_{max} is the maximum absorption observed for each organ of the individual. Gastrolith I_{max} was always measured on the day of ecdysis; cuticle I_{max} was determined on the first or second day of the premolt stage. "Relative gastrolith build-up time" (T_{GB}) was calculated by normalizing the time required for each animal to reach ecdysis, multiplied by 10. Similarly, the "relative gastrolith degradation time" (T_{GD}) was normalized for each individual, multiplied by 2.3, and added to the buildup scale, starting at 11. The ratio 10:2.3 represents the average ratio of the durations of gastrolith buildup and degradation (gastrolith buildup lasted an average of 15.45 days from induction to ecdysis, and gastrolith dissolution continued an average of 3.55 days after ecdysis).

Fourier transform infrared spectroscopy

FTIR spectroscopic analysis of the cuticle and gastrolith were performed on a Bruker (Fourier transform spectrometer) equipped with a DTGS detector. Samples were prepared by carefully removing cell debris and external organic layers by light mechanical scraping under excess running water. All samples were ground into powder in an agate mortar with a pestle. Samples with high organic content were immersed in liquid nitrogen during grinding to increase their brittleness. Clean samples were prepared in KBr pellets for spectroscopy. The work of Ajikumar *et al.* (2005) served as our reference, to which our FTIR findings were compared.

Scanning electron microscope

Mineralized cuticle and gastrolith samples were prepared for SEM inspection by rinsing in water and drying in air. Dry samples were dipped in liquid N_2 and broken. Broken sections were inspected after gold sputtering by an SEM FEI Quanta 200 scanning electron microscope at an acceleration voltage of 10–15 kV.

Histological gastrolith preparation

The gastrolith epithelial disc was surgically removed from intermolt crayfish 3 days after endocrine induction. Tissue samples were fixed in modified Carnoy II for 48 h and dehydrated gradually in an alcohol series. Tissues were cleared and embedded in Paraplast (Kendall, MA, USA) according to conventional procedures. Sections of 5 μm were cut and mounted on silane-coated slides (Menzel-Gläser, Braunschweig, Germany) and stained with hematoxylin and eosin.

In vitro *measurements at the gastrolith mineralization site*

Ca^{2+} and pH were determined with ion-specific microelectrodes that we built for our experiments. The potential difference between the reference electrode (a calomel reference electrode, Radiometer 401, Denmark) and the ion-specific microelectrode was measured with a high-impedance mV meter (Mascom, Germany). The data were collected with an AD card (National Instruments) and saved on a personal computer. Using this system, we measured ion activities rather than concentration. For measurement of Ca^{2+} activity, a Fluka 21193 calcium II ionophore (Tsien and Rink, 1980; Anker *et al.*, 1981) was used. The tip diameter was 1–10 μm, and the detection limit was 0.1 μmol l^{-1} in fresh water (Ammann, 1986). The Ca^{2+} microelectrode was calibrated in Ca^{2+} buffer solutions (1 and 10 mmol l^{-1}) with added background ions (basically similar to seawater with a practical salinity of about $S = 17$) to match the ionic composition of the organism's hemolymph. For measurements of H^+ concentrations, the microelectrode was based on an ionophore III liquid ion-exchange membrane (Fluka 60591) with a measuring range of pH 3–11 (de Beer *et al.*, 1997), commonly used for physiological studies (Boudreau and Jorgensen, 2001). The tip diameter of the microelectrode was 1–10 μm and the response time was fast. The lifetime of these sensors was typically 1 to 2 days. The pH microelectrode was calibrated in pH buffer solutions (Mettler Toledo, pH 4.01, 7.0, and 9.21) at a room temperature of 25 °C.

Before the measurements were made, the gastroliths were

surgically exposed. During the measurements, the crayfish was held in water to keep it alive. By means of micromanipulators, the pH and calcium microelectrodes were inserted into the cavity between the gastrolith disc epithelium and the cardiac stomach wall in a direction tangential to the gastrolith surface. Reference measurements were taken in a muscle and in the stomach cavity. Multiple pH and [Ca^{2+}] measurements were taken simultaneously from each individual at each location. Measurement duration for all five animals was 0.5 to 3 min.

Results

Changes in cuticle and gastrolith mineralization during the molt cycle are presented in Figure 1 as the intensities calculated from digital X-ray radiographs. The measured intensities are normalized with respect to the maximum absorbed intensity for each individual.

The initial increase in gastrolith intensity was observed at a relative gastrolith build-up time of 2 ($T_{GB} = 2$) and continued at an approximately linear rate to peak at ecdysis (Fig. 1A). Concurrently, the density of the cuticle remained almost constant during most of the premolt stage, but as ecdysis approached, a sharp decrease in cuticle density was detected at $T_{GB} = 8$. During the postmolt stage, at a relative gastrolith digestion time of 11 ($T_{GD} = 11$), the gastrolith rapidly degraded in the stomach, resulting in a sharp decrease in gastrolith intensity, and a corresponding increase in intensity was detected in the cuticle.

Figure 1B depicts digitized, intensity-based projections of gastrolith X-ray radiographs during five distinct molt stages. At $T_{GB} = 0$, prior to induction, no sign of calcification was evident. At a T_{GB} of 5.8 after induction, during premolt, small gastroliths could be observed. At $T_{GB} = 9.2$, the gastroliths attained their maximum, pre-ecdysis size. At $T_{GD} = 11.8$, immediately after ecdysis during postmolt, the gastroliths had already collapsed into the stomach and their digestion was under way, but the X-ray absorption images still show full-size gastroliths At T_{GD}=13.3, however, when gastrolith digestion was complete, gastroliths are no longer visible in the X-ray radiographs.

Figure 1B reflects the changes in cuticle absorption depicted in Figure 1A. Prior to molt induction (day −12), during the intermolt stage, the cuticle appeared to be smooth. As the premolt progressed, the texture of the cuticle became rougher. On day −1, numerous valleys were visible, representing changes in cuticle density levels that are also apparent in the decreased integrated density levels in Figure 1A. At day +3, during postmolt, the nearly constant cuticle density level was similar to that of day −12, prior to molt induction during intermolt.

Changes in the relative mineral contents in the cuticle and gastroliths during the molt cycle stages were followed with FTIR (Fig. 2). The unique absorption spectrum of ACC is characterized by a peak at 866 cm^{-1} (out-of-plane stretching), a split asymmetric peak at 1420–1474 cm^{-1}, and a strong broad asymmetric peak at 1080 cm^{-1} (solid lines, Fig. 2). Chitin is characterized by a distinct peak at 1650 cm^{-1} (Addadi *et al.*, 2003). Analyses of the FTIR spectra of the mineralized cuticle during intermolt and premolt and of the exuvia (Fig. 2A) reveal the peaks characteristic of ACC and the characteristic chitin peak (Fig. 2A). In contrast, the FTIR spectrum of the cuticle during the postmolt stage demonstrates an absence of mineral, and only the characteristics of chitin are apparent (Fig. 2A).

The FTIR spectra of the calcified premolt gastrolith (Fig. 2B) shows the characteristic ACC peaks at 866 cm^{-1}, 1420–1474 cm^{-1}, and 1070 cm^{-1}, as well as a shoulder at 1650 cm^{-1}, indicating the presence of chitin. A very small peak at 713 cm^{-1} is visible at premolt gastrolith, indicating the presence of residual amounts of calcite. In contrast, the spectrum of the noncalcified intermolt gastrolith shows a sharp peak at 1650 cm^{-1}, indicating the presence of chitin, but no peaks characteristic of ACC are evident (Fig. 2B).

SEM micrographs of cuticle cross sections at the intermolt and premolt stages and of the exuvia demonstrate the extent of cuticle degradation during the molt cycle (Fig. 3A). SEM images of the intermolt cuticle reveal the epicuticle to be densely mineralized without clear compartmental divisions, forming a relatively impermeable protective layer throughout the molt cycle. The exocuticle was composed of densely packed blocky deposits of chitin and mineral. The endocuticle was composed of chitin "galleries" interconnected with transverse chitin filaments. The voids in the chitin galleries were filled in part with blocky mineral deposits. The innermost layer is the membranous layer, which is made of unmineralized, loosely arranged fibers of chitin. Mineralization of the intermolt endocuticle was not continuous—variations in calcification were observed in different regions. Alternate regions of the endocuticle, 20–30 μm in scale in the lateral dimension and spanning most of the endocuticle thickness, remain mostly unmineralized. A higher magnification micrograph shows dense calcification in the interconnected laminated organic matrix (Fig. 3B).

During the premolt stage, the endocuticle and parts of the exocuticle were gradually degraded, a process that was initiated in the less mineralized segments of the cuticle. SEM examination showed that the degrading endocuticle mineral appeared to be washed-out, and the mineral blocky units (Fig. 3A, left arrow) and the chitinous regions were partially dissolved (Fig. 3A, right arrow). The higher magnification micrograph shows massive degradation of the mineral and the organic matrix during premolt (Fig. 3B, premolt and exuvia), whereas degradation was hardly observed during intermolt (Fig. 3B, intermolt).

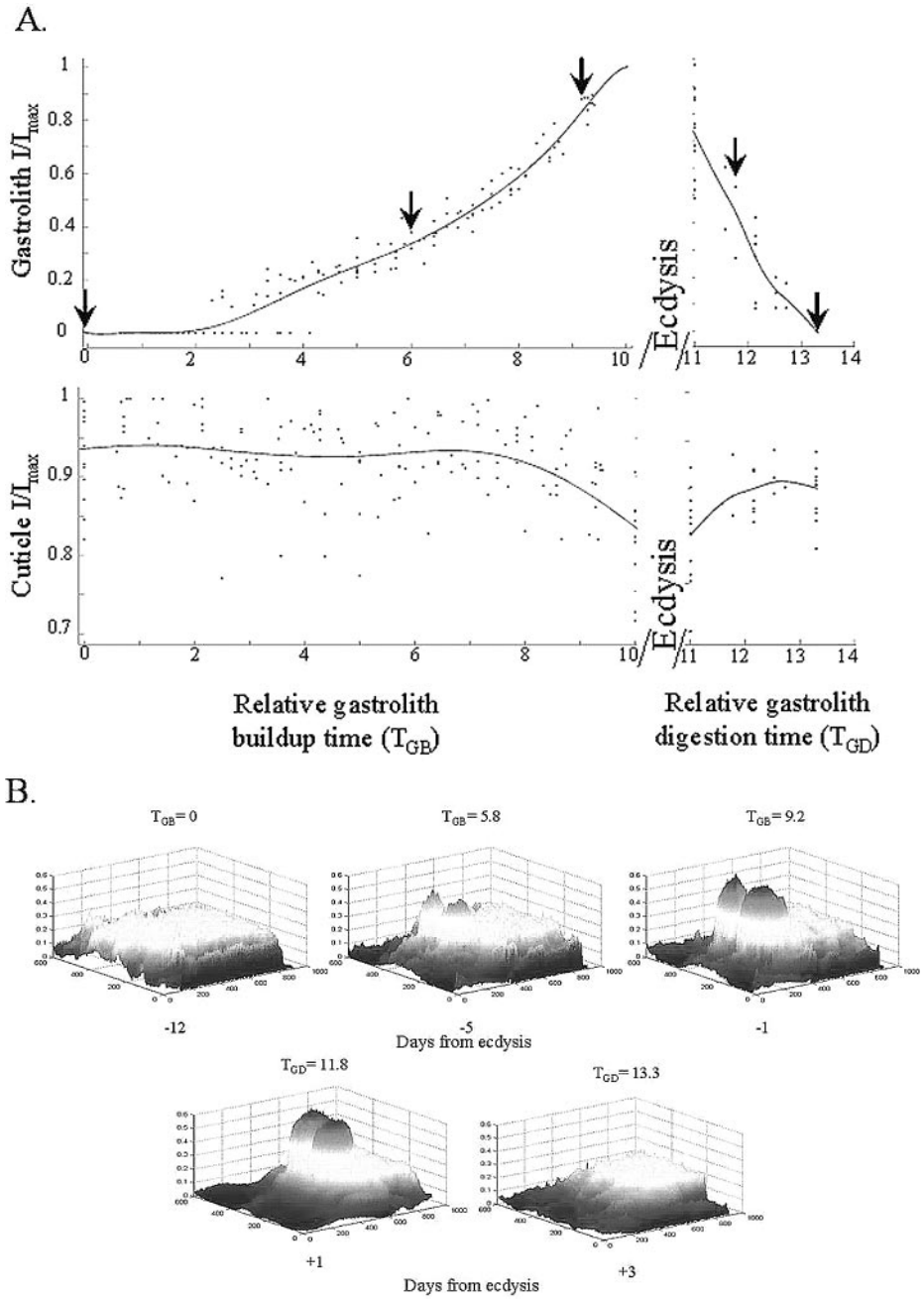

Figure 1. Dynamics of calcium mobilization during the molt cycle of *Cherax quadricarinatus*. (A) Absorption patterns of the gastrolith and cuticle during the molt cycle. I/I_{max} represents a calculated ratio of each animal's X-ray absorption during the different molt stages, normalized to the maximum absorption observed for each organ. Left: relative gastrolith build-up time (T_{GB}) was calculated for the periods between endocrine induction and ecdysis. Right: relative gastrolith digestion time (T_{GD}) was calculated from ecdysis to the total digestion of the gastrolith. Data were normalized according to the total number of days required for each individual. (B) Three-dimensional X-ray opacity patterns of the gastrolith in a representative individual during five distinct stages of the molt cycle. The images were taken at days $-12, -5, -1, +1$, and $+3$ from ecdysis, with the corresponding relative times indicated on top (black arrows). The *x* and *y* axes indicate the projection of the gastrolith onto the imaging plane; the *z* axis is the X-ray opacity level.

Demineralization and degradation of the chitin matrix did not progress equally in all the cuticle regions: in some places, the matrix remained almost fully mineralized, with nondegraded zones being adjacent to degraded zones, the latter spanning roughly 20 μm. As the molt cycle progressed, voluminous caverns devoid of both the mineral and

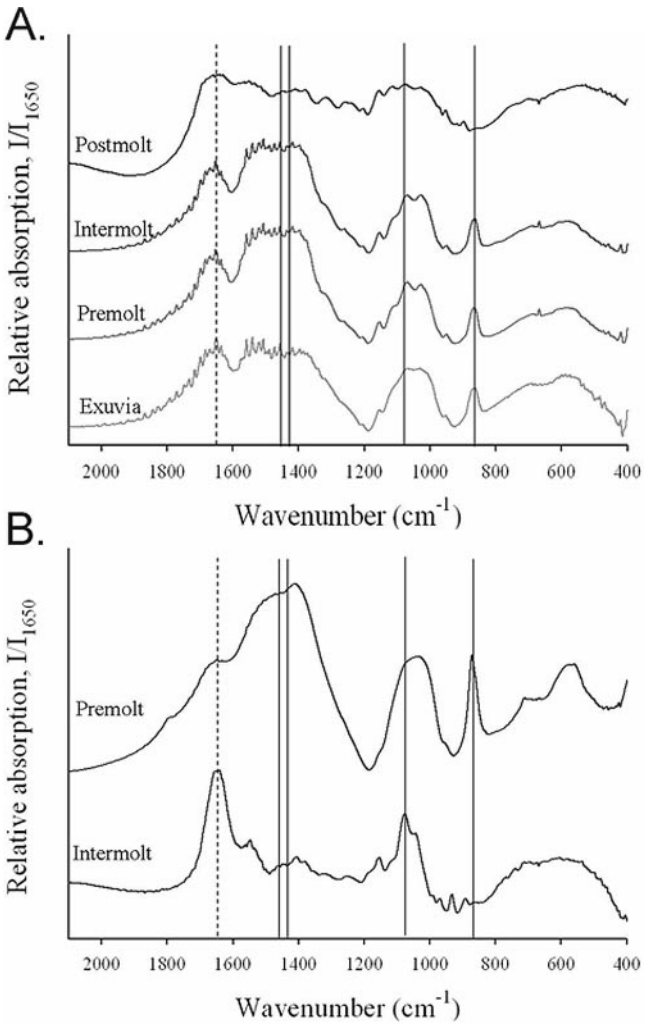

Figure 2. Changes in Fourier transform infrared spectroscopy (FTIR) spectra of the cuticle and gastrolith during the molt cycle in *Cherax quadricarinatus*. Solid vertical lines represent the main peaks in the vibrational spectrum of amorphous calcium carbonate (866, 1080, 1420–1474 cm^{-1}). The dashed vertical line represents the main chitin peak (1650 cm^{-1}). For purposes of comparison, the results were normalized with respect to chitin absorption at 1650 cm^{-1}. (A) FTIR spectra of the cuticle during four distinct molt stages. From top to bottom: postmolt, intermolt, premolt, and exuvia. (B) FTIR spectra of premolt calcified gastrolith and intermolt noncalcified gastrolith.

the organic matrix framework were formed (Fig. 3A in exuvia). The molt cycle culminates in ecdysis, during which the exuvia, comprising the remains of the mineralized organic matrix, is discarded. Remarkably, in the exuvia, the epicuticle remained fully mineralized. Massive decalcification was revealed in the endocuticle and parts of the exocuticle (Fig. 3A).

Gastrolith ultrastructure was characterized by alternating layers of organic matrix and mineral. The SEM micrographs of the gastrolith during early premolt (Fig. 4A–D) show the onset of mineralization and the initiation of layering. The surface of the top layer shows mineral-free chitin threads interspersed sporadically with ACC spherules 40 to 50 nm in size (Fig. 4A). Figure 4B reveals a more developed structure comprising a layer of chitinous threads covering a layer of dense ACC spherules. We suspect that the embossed circular patterns on the gastrolith's external layer (Fig. 4C) represent epithelial cell outlines forming tissue together with chitinous threads and sporadically distributed ACC spherules. Figure 4D presents an area of the lightly mineralized gastrolith showing the compact, mostly nonmineralized structure of the matrix and the interconnected chitinous threads.

SEM micrographs of a premolt mineralized gastrolith are presented in Figure 4E–H. The fractured gastrolith layer (outer surface and the cross section) shown in Figure 4E exhibits the same embossed patterns evident in Figure 4C. Figure 4F reveals a layer of organic material separating several dense layers, some of which show tightly packed ACC spherules. A cross section of an area of ACC layers of different densities is shown (Fig. 4G). At lower magnification (Fig. 4H), the gastrolith has a steplike fractured appearance. Figure 4I is a light micrograph of a pair of late premolt gastroliths taken from the same animal. The gastrolith on the left was demineralized, leaving only the organic matrix, whereas that on the right is intact. The figure clearly shows that the demineralized organic matrix retains its integrity and its original shape, which is identical to that of the intact gastrolith. SEM micrographs of a fractured surface (Fig. 4J) and a cross section (Fig. 4K) of a gastrolith in the late premolt stage reveal onionlike structures of concentric mineral layers separated by lower density layers that probably contain more organic material.

Histological sections of a gastrolith disc during early premolt (Fig. 5A–D) show that the disc comprises the stomach wall, an outer layer of columnar epithelium disc, and the cavity between them where the gastrolith is formed. At low magnification, the gastrolith disc shows the stomach cavity and the initial arrangement of the chitin in the newly formed gastrolith (Fig. 5A). At the junction between the stomach wall and the outer epithelial layer, two types of surface epithelial tissues are observed—an inner layer composed of squamous epithelium that covers the stomach wall and the outer layer comprising columnar epithelium (Fig. 5B). At a higher magnification, it may be seen that the outer epithelium layer comprises a single layer of columnar invaginating cells branching at their apical portions (Fig. 5C). The thin, chitinous layer forming the early gastrolith is observed at high magnification in Figure 5D.

In situ pH and [Ca^{2+}] were measured in three areas near the gastrolith disc (see Fig. 5A–D); the gastrolith cavity (between the stomach wall and the epithelial disc), the stomach, and adjacent muscle; values are reported in Figure 5E. No significant changes in calcium concentration were observed at the three measurement sites, with calcium concentrations ranging

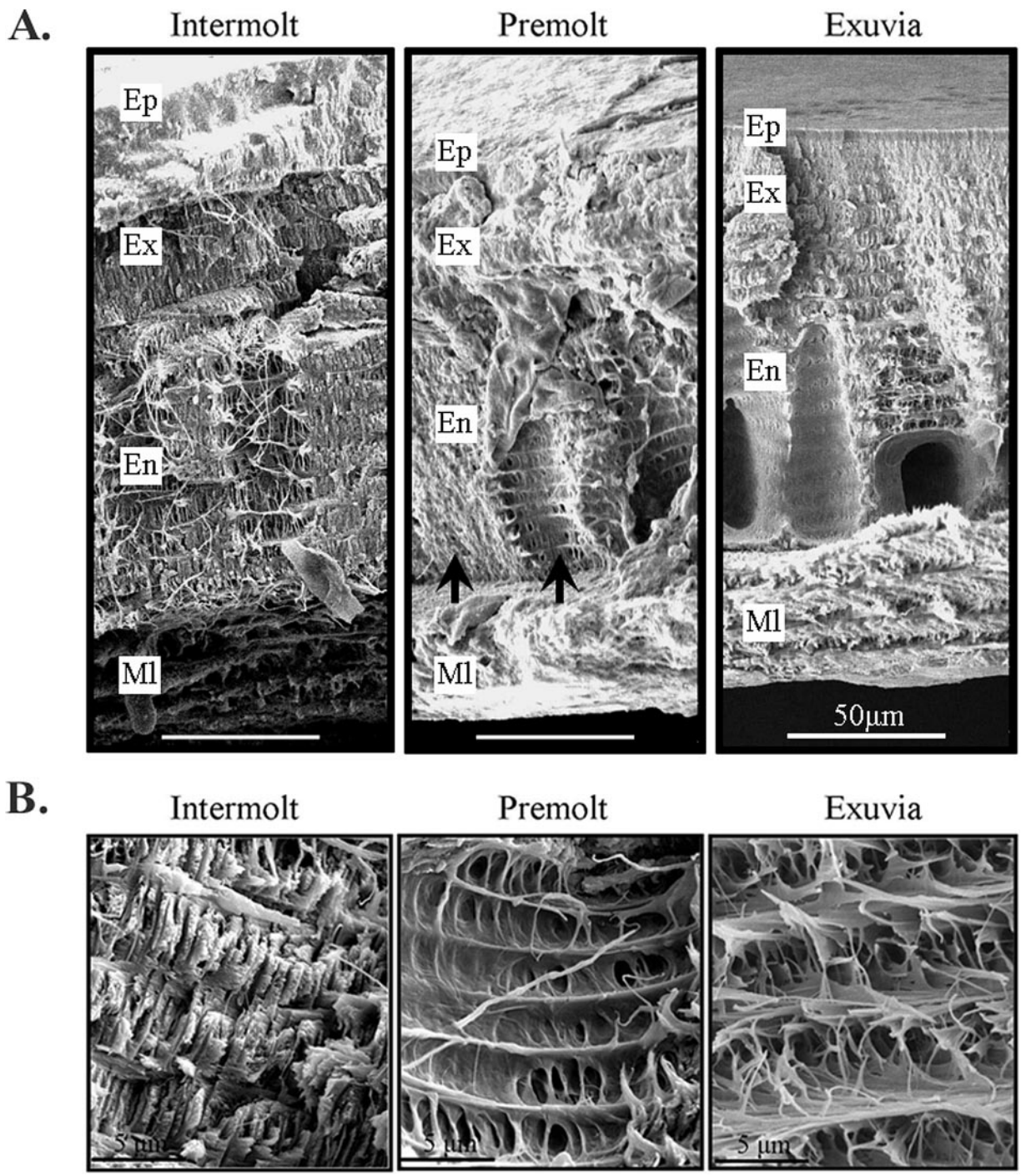

Figure 3. Changes in mineralization patterns of intermolt and premolt cuticles, and of exuvia in *Cherax quadricarinatus*. (A) Low-magnification SEM micrographs of cuticle cross sections. Ep, epicuticle; Ex, exocuticle; En, endocuticle; Ml, membranous layer. (B) High-magnification SEM micrographs of representative areas demonstrating matrix structure and mineral deposition in the cuticle during three stages of the molt cycle.

from 10–11 mmol l^{-1}. On the other hand, pH levels were markedly different at each of the measurement sites, with gastrolith levels ranging from 8.5 to 8.8, muscle levels from 7.5 to 7.9 and stomach levels from 6.6 to 7.4.

Discussion

In this study we followed the inverse dynamics of cuticle and gastrolith calcification during the *Cherax quadricari-*

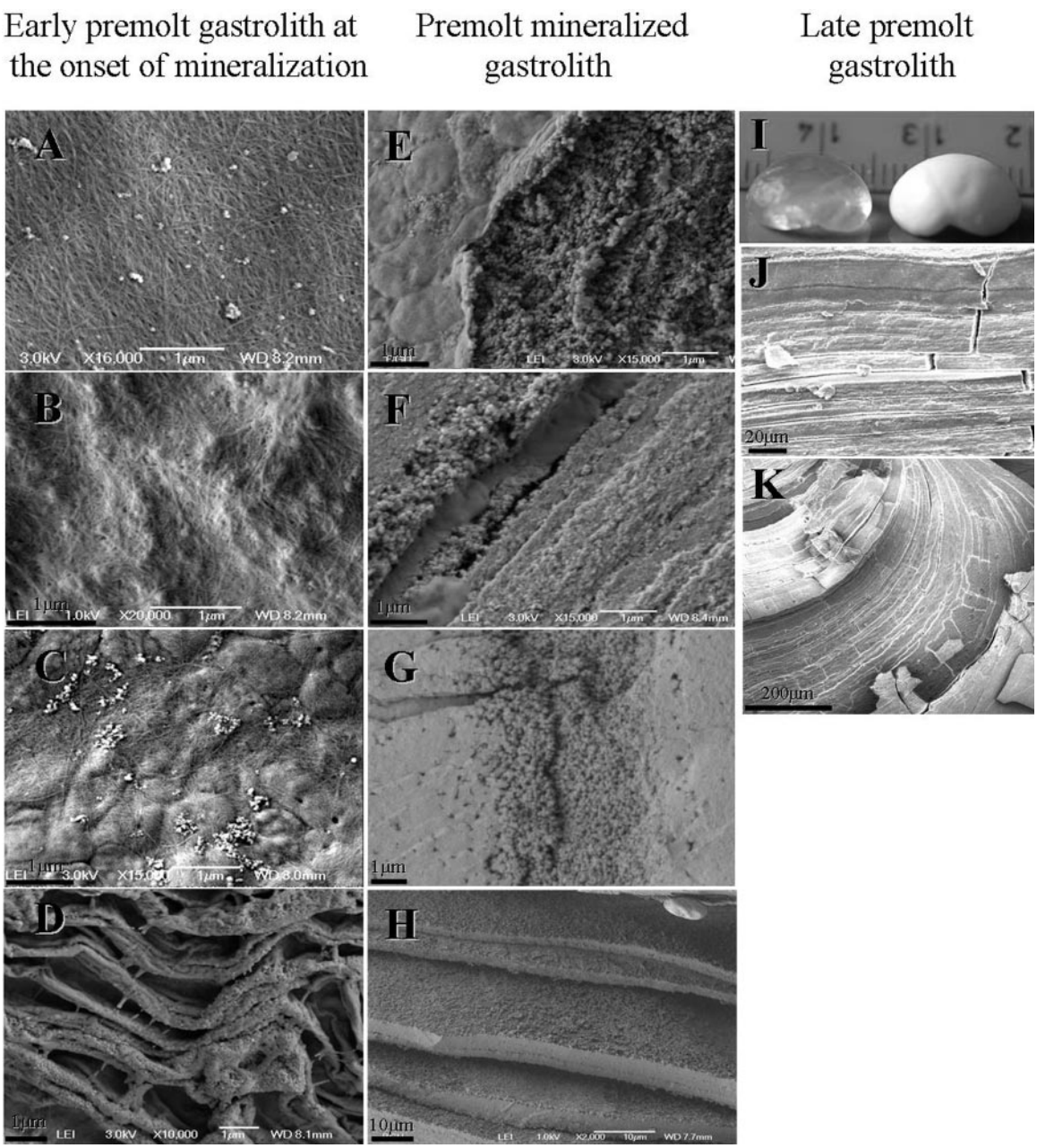

Figure 4. Spatial structures of the biological matrix and mineral in the gastrolith of *Cherax quadricarinatus*. Left column: SEM micrographs of early premolt gastroliths at the onset of mineralization. (A) Lightly mineralized chitinous biological matrix showing sporadic organization of amorphous calcium carbonate (ACC) spherules. (B) Biological chitinous matrix covering of ACC spherules. (C) Biological chitinous matrix with sporadic ACC spherules showing the suggested embossed cell outlines of the epithelial forming tissue. (D) Area of compact, mostly unmineralized, biological matrix. Middle column: SEM micrographs of premolt mineralized gastroliths. (E) A fractured gastrolith layer showing both the proposed embossed cell outlines and a cross section of dense ACC spherules. (F) Cross section showing preliminary organization of layers with differential covering of organic material on the ACC spherules. (G) Cross section showing differences in organic material covering of the ACC spherules. (H) Low-magnification gastrolith cross section showing typical gastrolith layering. Right column: images of late premolt gastroliths. (I) Images of two gastroliths from a single late premolt individual: intact gastrolith (right) and a demineralized gastrolith (left) showing the spatial shape of the chitinous biological matrix. (J) SEM micrographs showing the concentric organization of alternating organic matrix and mineral layers. (K) Higher magnification of SEM micrographs showing a section of the gastrolith fracture.

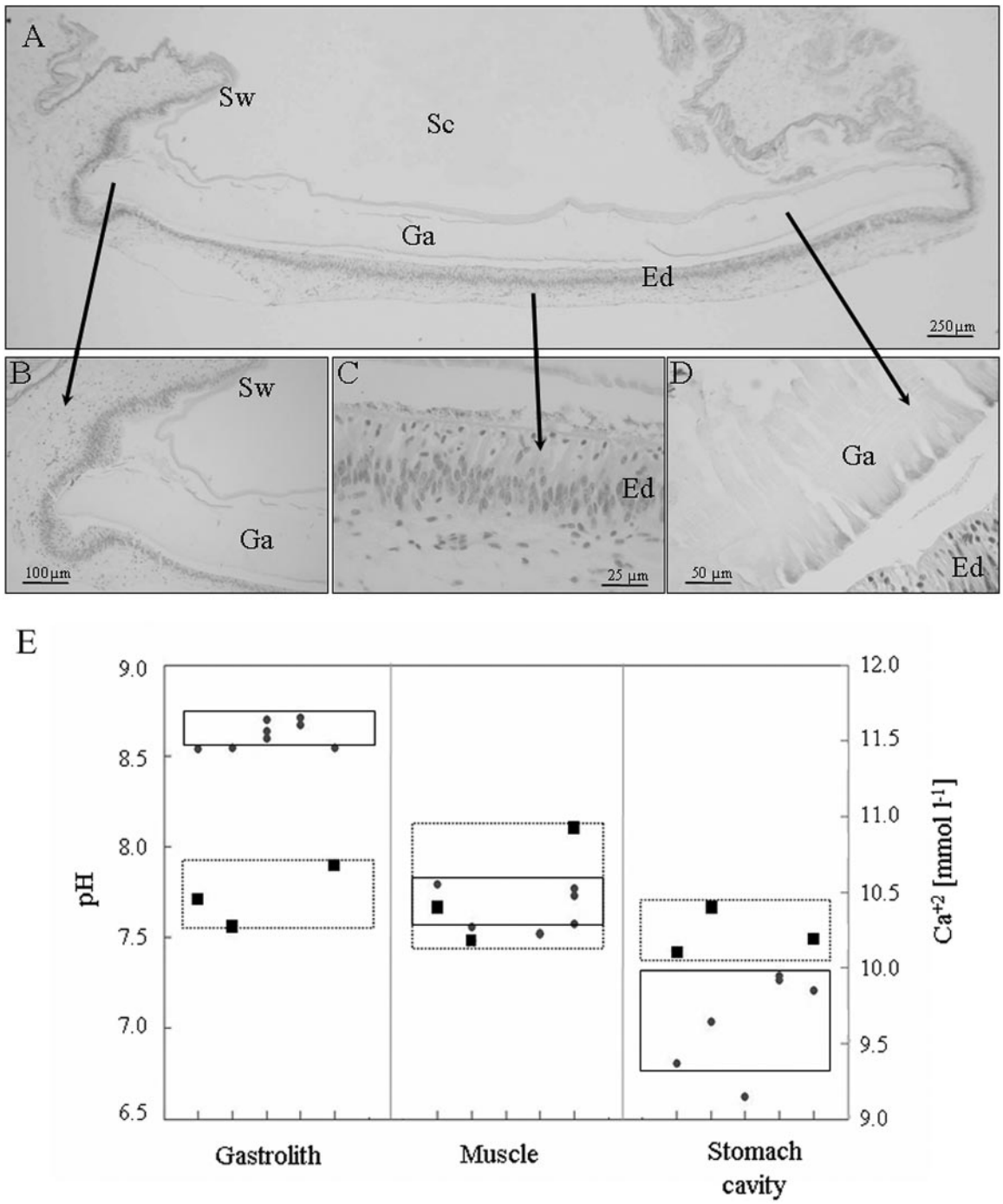

Figure 5. The gastrolith biomineralization site, which includes the gastrolith, its epithelial disc, the stomach wall, and the stomach cavity. Calcium and pH measurements in these areas in a premolt *Cherax quadricarinatus*. (A) Low-magnification light micrograph of the stomach cavity (Sc) and wall (Sw), including an entire early premolt gastrolith (Ga) and its epithelial disc (Ed), stained in hematoxylin and eosin. (B) Higher magnification of the junction between the stomach wall and the gastrolith epithelial disc. (C) Higher magnification of a representative section of columnar epithelial disc cells. (D) Higher magnification showing the layered structure of the gastrolith. (E) Calcium concentration in mmol l^{-1} (squares) and pH (filled circles) in the gastrolith/epithelial disc space, in adjacent muscle, and in the stomach cavity of a premolt *C. quadricarinatus* crayfish. Boxes with solid lines enclose similar pH measurements. Dashed-line boxes enclose similar calcium concentration measurements. Boxes are centered at the numerical average value; the box height is the calculated standard deviation. Each tick on the *x* axis represents a sampled individual.

natus molt cycle by using changes in their respective densities as observed in X-ray digital radiographs. The changes in density accurately reflect the relative mineral content in each calcification site and, therefore, provide an accurate tool for assessing the calcification state in the living animal. The rapid accumulation of mineral in the gastrolith during premolt is manifested by a simultaneous increase in gastrolith density and a decrease in cuticle density prior to ecdysis. These two processes represent the reabsorption of calcium from the degraded cuticle and its deposition in the gastrolith.

Changes in mineral content of the calcification sites represent only relatively small fractions of the crayfish's entire dynamic store of calcium. In fact, the relatively minor decrease in cuticle mineral content during premolt does not reflect the maximum crayfish potential for calcium reabsorption, which can account for up to 50% of the body's total calcium content (Wheatly and Ayers, 1995). And although the gastrolith shows dramatic changes in mineral content during premolt, those changes correspond to only about 10% of the body's total calcium content (Aiken and Waddy, 1992). The remaining greater part of the calcium is excreted through the gills or lost in the exuvia (Wheatly and Gannon, 1995).

Because most of the reabsorbed calcium is excreted and not stored, premolt reabsorption must serve primarily to weaken the cuticle in preparation for shedding (Wheatly and Gannon, 1995). The differences between the density changes at the two calcification sites and their relative contributions to the body's total calcium content result from the size differences of the two sites. During postmolt, rapid digestion of the gastrolith in the stomach takes place concurrently with the calcification of the new, hardening cuticle. However, the changes in cuticle density cannot be explained by the supply of calcium from the gastrolith alone, since the latter provides a mere 4%–15% of the total needed for cuticle calcification (Wheatly and Gannon, 1995). The remaining calcium required to complete calcification must be supplied exogenously, mostly by branchial uptake (Wheatly, 1999).

Cuticle mineral content has been studied in many crustacean species, in all of which calcium carbonate constitutes the main calcification mineral (Greenaway, 1985; Wheatly and Ayers, 1995; Luquet and Marin, 2004). Various studies identified the polymorphic form of calcium carbonate in the cuticles of different crustacean species as crystalline calcite (Stevenson, 1985; Lowenstam and Weiner, 1989; Pratoomchat *et al.*, 2002), as amorphous calcium carbonate (ACC) (Levi-Kalisman *et al.*, 2002), or as a coexistence of the two (Aiken and Waddy, 1992; Becker *et al.*, 2005; Sugawara *et al.*, 2006). Studies of the crab *Callinectes sapidus* (Dillaman *et al.*, 2005) and of the giant prawn *Macrobrachium rosenbergii* (Soejoko and Tjia, 2003) along with several reports on species other than crustaceans postulated that the amorphous form may serve as the precursor of the crystalline form (Aizenberg *et al.*, 1996). Our findings suggest that stable ACC is the principal form of calcium carbonate in the cuticle of *C. quadricarinatus*. These results were confirmed with Raman spectroscopy (data not shown).

Although earlier reports suggested that the predominant mineral polymorph of the gastrolith is calcite (Ueno, 1980), our findings concur with reports that ACC is the main polymorph (Travis, 1963c). ACC was also reported as the main polymorph for transient calcium deposits in other crustacean species (Raz *et al.*, 2002; Becker *et al.*, 2003). The observation that ACC is the main polymorph in both the gastroliths and the cuticle may be related to its higher solubility, which enables the rapid dissolution necessary for the mobilization of calcium during the periodic molt cycle.

SEM images of *C. quadricarinatus* cuticles during intermolt and premolt and of the exuvia show four distinct cuticular layers. The calcification of the cuticle during postmolt (except for the exuvia) was not examined in this study. The mineralized horizontal helical arrangement of chitin in the exoskeleton during intermolt is similar to that in a number of crustacean species (Arsenault *et al.*, 1984; Roer and Dillaman, 1984; Becker *et al.*, 2003). However, the vertical cytoplasmic extensions of the epidermal layer previously described in lobsters (Arsenault *et al.*, 1984) were not detected in our SEM images of the cuticle. As was found in the crab *Callinectes sapidus* (Roer and Dillaman, 1984) and other crayfish species such as *Orconectes virilis* (Travis, 1965; Lowenstam and Weiner, 1989), the endocuticle in *C. quadricarinatus* seems to be the thickest of the four layers. In *C. quadricarinatus*, the endocuticle undergoes massive degradation of the mineral and organic material (as can be observed in the premolt and exuvia samples), with the epicuticle remaining calcified with no apparent changes and the exocuticle undergoing partial degradation.

Most of the studies performed on gastroliths in the last 25 years have focused on the gastrolith disc epithelium and its unique mechanism for calcium transport (Ueno, 1980; Ueno and Mizuhira, 1983, 1984; Ueno *et al.*, 1992). To the best of our knowledge, SEM images have never been recorded during gastrolith calcification, and therefore, our study is comparable only with the transmission electron micrographs and light micrographs of Travis in the crayfish *Orconectes virilis* Hagen (Travis, 1960, 1963c; Travis and Friberg, 1963a). In her work, Travis describes the gastroliths as a calcified layer containing particles of 30 to 70 nm in size that lack well-defined shapes and are embedded in a loose, fibrous meshwork. Travis was the first to suggest that the calcium carbonate is stored in the gastrolith in a poorly crystalline state and not as calcite. The findings of Travis coincide with our SEM images of the early premolt, lightly mineralized gastrolith, where such fibers and sporadic ACC spherules ranging in size from 40 to 60 nm are evident (as seen in Fig. 4E). The description of the lamellae and crystals

of the "old and thick portion of the gastrolith" reported by Travis resemble the lamellar section of the gastrolith as observed in our study in the early premolt (at the onset of mineralization) and late premolt gastroliths (Fig. 4H and J).

Little is known about the conditions needed for the precipitation of the mineral in the gastrolith or in any other transient calcium deposits in crustaceans. Therefore, they are assumed to be similar to the widely investigated conditions required for cuticular calcification in decapod crustaceans. One assumption is that mineral deposition is mediated by electrical action between quinine-protein complexes and the calcifying regions in response to the generation of a pH gradient (Digby, 1964; Aiken and Waddy, 1992). It is also believed that carbonic anhydrase is the key regulator of pH at the site of calcification (Aiken and Waddy, 1992), although epithelial proton ATPases may also contribute to pH (Zare and Greenaway, 1998). The importance of pH in mineral dissolution or calcification was demonstrated in the cuticle of the crab *Callinectes sapidus,* where a slight decrease in pH resulted in the dissolution of salts from the carapace into their ionic components. On the other hand, a slight increase in pH resulted in the formation of calcium carbonate on the inner face of the cuticle (Cameron, 1985). Calcium carbonate exchange between the cuticle and the hemolymph to facilitate carbonate availability is also influenced by pH (Cameron, 1985). In our study, the higher pH measured in the gastrolith pouch vis-à-vis the other sites tested may be an essential factor for the formation of calcium carbonate (Addadi *et al.*, 2003). Addadi and her coworkers (2003) suggested that OH^- ions actively participate in the stabilization of the amorphous phase. Nevertheless, the common view is that the formation and stabilization of the amorphous calcium carbonate requires other factors, probably macromolecules such as specialized proteins (Aizenberg *et al.*, 2002) or ions such as magnesium (Aizenberg *et al.*, 2002), both acting as crystallization inhibitors.

In our study, calcium measurements in all tested sites indicated that the concentration remained constant at an average level of approximately 10 mmol l^{-1}, similar to the hemolymph levels reported in the literature (Wheatly and Gannon, 1995). Although *C. quadricarinatus* is a freshwater crayfish, the measured calcium concentration of 10 mmol l^{-1} is similar to that found in seawater (Greenaway, 1985). One can assume that the massive calcium mobilization transferred through the hemolymph during premolt (Greenaway, 1985) results in a dramatic increase in hemolymph Ca^{+2} concentration, as observed in terrestrial isopods (Ziegler *et al.*, 2000). However, the maintenance of a constant Ca^{+2} levels should be investigated further in light of reports of sharp increases in the levels of protein-bound calcium in crayfish hemolymph during premolt (McWhinnie, 1962; McWhinnie *et al.*, 1969).

Using our model organism of a decapod crustacean, further research on the mechanisms and conditions of calcium carbonate precipitation in temporary deposits, together with the identification of the elements stabilizing ACC, is needed for a deeper understanding of this complex process.

Acknowledgments

The technical assistance and animal husbandry by Mr. Liron Friedman are highly appreciated. This research was supported in part by a grant from Amorphical Ltd. through B.G. Negev Ltd. We thank Mr. Patrick Martin for styling the manuscript. We would also like to thank Dr. E. Barnea for allowing us to perform the preliminary X-ray experiments in his clinic.

Literature Cited

Addadi, L., S. Raz, and S. Weiner. 2003. Taking advantage of disorder: amorphous calcium carbonate and its roles in biomineralization. *Adv. Mater.* **15:** 959–970.

Ahearn, G. A., P. K. Mandal, and A. Mandal. 2004. Calcium regulation in crustaceans during the molt cycle: a review and update. *Comp. Biochem. Physiol. A Mol. Integr. Physiol.* **137:** 247–257.

Aiken, D. E., and S. L. Waddy. 1992. The growth-process in crayfish. *Rev. Aquat. Sci.* **6:** 335–381.

Aizenberg, J., G. Lambert, L. Addadi, and S. Weiner. 1996. Stabilization of amorphous calcium carbonate by specialized macromolecules in biological and synthetic precipitates. *Adv. Mater.* **8**: 222–226.

Aizenberg, J., G. Lambert, S. Weiner, and L. Addadi. 2002. Factors involved in the formation of amorphous and crystalline calcium carbonate: a study of an ascidian skeleton. *J. Am. Chem. Soc.* **124**: 32–39.

Ajikumar, P. K., L. G. Wong, G. Subramanyam, R. Lakshminarayanan, and S. Valiyaveettil. 2005. Synthesis and characterization of monodispersed spheres of amorphous calcium carbonate and calcite spherules. *Cryst. Growth Des.* **5**: 1129–1134.

Al-Horani, F. A., S. M. Al-Moghrabi, and D. de Beer. 2003. The mechanism of calcification and its relation to photosynthesis and respiration in the scleractinian coral *Galaxea fascicularis*. *Mar. Biol. (Berlin)* **142**: 419–426.

Ammann, D. 1986. *Ion-Selective Microelectrodes, Principles, Design and Application.* Springer-Verlag, Berlin.

Anker, P., E. Wieland, D. Ammann, R. E. Dohner, R. Asper, and W. Simon. 1981. Neutral carrier based ion-selective electrode for the determination of total calcium in blood serum. *Anal. Chem.* **53**: 1970–1974.

Arsenault, A. L., J. D. Castell, and F. P. Ottensmeyer. 1984. The dynamics of exoskeletal-epidermal structure during molt in juvenile lobster by electron-microscopy and electron spectroscopic imaging. *Tissue Cell* **16:** 93–106.

Becker, A., U. Bismayer, M. Epple, H. Fabritius, B. Hasse, J. M. Shi, and A. Ziegler. 2003. Structural characterisation of x-ray amorphous calcium carbonate (ACC) in sternal deposits of the crustacea *Porcellio scaber*. *Dalton Trans.* **2003:** 551–555.

Becker, A., A. Ziegler, and M. Epple. 2005. The mineral phase in the cuticles of two species of Crustacea consists of magnesium calcite, amorphous calcium carbonate, and amorphous calcium phosphate. *Dalton Trans.* **2005:** 1814–1820.

Boudreau, P. B., and B. Jorgensen. 2001. *The Benthic Boundary Layer: Transport Processes and Biogeochemistry.* Oxford University Press, New York.

Cameron, J. N. 1985. Post-moult calcification in the blue crab (*Callinectes sapidus*): relationships between apparent net H^+ excretion, calcium and bicarbonate. *J. Exp. Biol.* **119:** 275–285.

de Beer, D., A. Glud, E. Epping, and M. Kuhl. 1997. A fast-responding CO^2 microelectrode for profiling sediments, microbial mats, and biofilms. *Limnol. Oceanogr.* **42:** 1590–1600.

Digby, P. S. B. 1964. The mechanism of calcification in crustacean cuticle. *Proc. Physiol. Soc.* **6:** 29–30.

Dillaman, R., S. Hequembourg, and M. Gay. 2005. Early pattern of calcification in the dorsal carapace of the blue crab, *Callinectes sapidus*. *J. Morphol.* **263:** 356–374.

Drach, P., and C. Tchernigovtzeff. 1967. Sur la méthode de détermination des stades d'intermue et son application générale aux crustacés. *Vie Milieu* **18:** 595–610.

Giraudguille, M. M. 1984. Fine structure of the chitin protein system in the crab cuticle. *Tissue Cell* **16:** 75–92.

Greenaway, P. 1985. Calcium balance and moulting in the crustacea. *Biol. Rev. Camb. Philos. Soc.* **60:** 425–454.

Hartnoll, R. G. 1982. Growth. Pp. 111–197 in *The Biology of Crustacea*, D. E. Bliss, ed. Academic Press, New York.

Levi-Kalisman, Y., S. Raz, S. Weiner, L. Addadi, and I. Sagi. 2002. Structural differences between biogenic amorphous calcium carbonate phases using x-ray absorption spectroscopy. *Adv. Funct. Mater.* **12:** 43–48.

Lowenstam, H. A., and S. Weiner. 1989. *On Biomineralization.* Oxford University Press, New York.

Luquet, G., and F. Marin. 2004. Biomineralisations in crustaceans: storage strategies. *C.R. Palevol* **3:** 515–534.

McWhinnie, M. A. 1962. Gastrolith growth and calcium shifts in the freshwater crayfish, *Orconectes virilis*. *Comp. Biochem. Physiol.* **7:** 1–14.

McWhinnie, M. A., M. O. Cahoon, and R. Johanneck. 1969. Hormonal effects on calcium metabolism in Crustacea. *Am. Zool.* **9:** 841–855.

Nakatsuji, M. T., H. Keino, K. Tamura, S. Yoshimura, T. Kawakami, S. Aimoto, and H. Sonobe. 2000. Changes in the amounts of the molt-inhibiting hormone in the sinus gland during the molt cycle of the American crayfish, *Procambarus clarkii*. *Zool. Sci.* **17:** 1129–1136.

Pavey, C. R., and D. R. Fielder. 1990. Use of gastrolith development in molt staging the fresh-water crayfish *Cherax cuspidatus* Riek, 1969. *Crustaceana* **59:** 101–105.

Pratoomchat, B., P. Sawangwong, R. Guedes, M. D. Reis, and J. Machado. 2002. Cuticle ultrastructure changes in the crab *Scylla serrata* over the molt cycle. *J. Exp. Zool.* **293:** 414–426.

Rao, K. R., C. J. Mohrherr, D. Reinschmidt, and M. Fingerman. 1977. Gastrolith growth during proecdysis in crayfish, *Faxonella clypeata* (Hay, 1899) (Decapoda, Astacoidea). *Crustaceana* **32:** 256–264.

Raz, S., O. Testeniere, A. Hecker, S. Weiner, and G. Luquet. 2002. Stable amorphous calcium carbonate is the main component of the calcium storage structures of the crustacean *Orchestia cavimana*. *Biol. Bull.* **203:** 269–274.

Roer, R., and R. Dillaman. 1984. The structure and calcification of the crustacean cuticle. *Am. Zool.* **24:** 893–909.

Shechter, A., E. D. Aflalo, C. Davis, and A. Sagi. 2005. Expression of the reproductive female-specific vitellogenin gene in endocrinologically induced male and intersex *Cherax quadricarinatus* crayfish. *Biol. Reprod.* **73:** 72–79.

Shechter, A., M. Tom, Y. Yudkovski, S. Weil, S. A. Chang, E. S. Chang, V. Chalifa-Caspi, A. Berman, and A. Sagi. 2007. Search for hepatopancreatic ecdysteroid-responsive genes during the crayfish molt cycle: from a single gene to multigenicity. *J. Exp. Biol.* **210:** 3525–3537.

Soejoko, D. S., and M. O. Tjia. 2003. Infrared spectroscopy and x-ray diffraction study on the morphological variations of carbonate and phosphate compounds in giant prawn (*Macrobrachium rosenbergii*) skeletons during its moulting period. *J. Mater. Sci.* **38:** 2087–2093.

Stevenson, J. R. 1985. Dynamics of the integument. Pp. 2–42 in *The Biology of Crustacea*, D. R. Bliss and L. H. Mantel, eds. Acdemic Press, New York.

Sugawara, A., T. Nishimura, Y. Yamamoto, H. Inoue, H. Nagasawa, and T. Kato. 2006. Self-organization of oriented calcium carbonate/polymer composites: effects of a matrix peptide isolated from the exoskeleton of a crayfish. *Angew. Chem. Int. Ed.* **45:** 2876–2879.

Travis, D. F. 1960. The deposition of skeletal structures in the crustacea. I. The histology of the gastrolith skeletal tissue complex and the gastrolith in the crayfish, *Orconectes (Cambarus) virilis* Hagen —Decapoda. *Biol. Bull.* **118:** 137–149.

Travis, D. F. 1963a. The deposition of skeletal structures in the crustacea. 2. The histochemical changes associated with the development of the nonmineralized skeletal components of the gastrolith discs of the crayfish, *Orconectes virilis* Hagen. *Acta Histochem.* **15:** 251–268.

Travis, D. F. 1963b. The deposition of skeletal structures in the crustacea. 3.The histochemical changes associated with the development of the mineralized gastroliths in the crayfish, *Orconectes virilis* Hagen. *Acta Histochem.* **15:** 269–284.

Travis, D. F. 1963c. Structural features of mineralization from tissue to macromolecular levels of organization in the decapod crustacea. *Ann. N.Y. Acad. Sci.* **109:** 177–245.

Travis, D. F. 1965. The deposition of skeletal structures in the crustacea. 5. The histomorphological and histochemical changes associated with the development and calcification of the branchial exoskeleton in the crayfish, *Orconectes virilis* Hagen. *Acta Histochem.* **20:** 193–222.

Travis, D. F., and U. Friberg. 1963a. The deposition of skeletal structures in the crustacea. IV. Microradiographic studies of the gastrolith of the crayfish *Orconectes virilis* Hagen. *J. Ultrastruct. Res.* **8:** 48–65.

Travis, D. F., and U. Friberg. 1963b. The deposition of skeletal structures in the crustacea. VI. Microradiographic studies of the exoskeleton of the crayfish *Orconectes virilis* Hagen. *J. Ultrastruct. Res.* **59:** 285–301.

Tsien, R. Y., and T. J. Rink. 1980. Neutral carrier ion-selective microelectrodes for measurement of intracellular free calcium. *Biochim. Biophys. Acta* **599:** 623–638.

Ueno, M. 1980. Calcium-transport in crayfish gastrolith disk—morphology of gastrolith disk and ultrahistochemical demonstration of calcium. *J. Exp. Zool.* **213:** 161–171.

Ueno, M., and V. Mizuhira. 1983. Calcium-transport mechanism in crayfish gastrolith epithelium correlated with the molting cycle. 1. The demonstration of calcium-accumulating sites. *Acta Histochem. Cytochem.* **16:** 596–605.

Ueno, M., and V. Mizuhira. 1984. Calcium-transport mechanism in crayfish gastrolith epithelium correlated with the molting cycle. 2. Cytochemical demonstration of Ca^{2+}-ATPase and Mg^{2+}-ATPase. *Histochemistry* **80:** 213–217.

Ueno, M., H. J. Bidmon, and W. E. Stumpf. 1992. Ecdysteroid binding sites in gastrolith forming tissue and stomach during the molting cycle of crayfish *Procambarus clarkii*. *Histochemistry* **98:** 1–6.

Wheatly, M. G. 1999. Calcium homeostasis in Crustacea: the evolving role of branchial, renal, digestive and hypodermal epithelia. *J. Exp. Zool.* **283:** 620–640.

Wheatly, M. G., and J. Ayers. 1995. Scaling of calcium, inorganic contents, and organic contents to body-mass during the molting cycle of the fresh-water crayfish *Procambarus clarkii* (Girard). *J. Crustac. Biol.* **15:** 409–417.

Wheatly, M. G., and A. T. Gannon. 1995. Ion regulation in crayfish—fresh-water adaptations and the problem of molting. *Am. Zool.* **35:** 49–59.

Willig, A., and R. Keller. 1973. Molting hormone content, cuticle growth and gastrolith growth in the molt cycle of the crayfish *Orconectes limosus*. *J. Comp. Physiol.* **86:** 377–388.

Yano, I. 1975. An electron microscope study on the calcification of the exoskeleton in the shore crab. *Bull. Jpn. Soc. Fish. Oceanogr.* **41:** 1079–1082.

Zare, S., and P. Greenaway. 1998. The effect of moulting and sodium depletion on sodium transport and the activities of Na^+K^+-ATPase, and V-ATPase in the freshwater crayfish *Cherax destructor* (Crustacea : Parastacidae). *Comp. Biochem. Physiol. A Mol. Integr. Physiol.* **119:** 739–745.

Ziegler, A., T. Grospietsch, T. H. Carefoot, J. P. Danko, M. Zimmer, I. Zerbst-Boroffka, and S. C. Pennings. 2000. Hemolymph ion composition and volume changes in the supralittoral isopod *Ligia pallasii* Brandt, during molt. *J. Comp. Physiol. B Biochem. Syst. Environ. Physiol.* **170:** 329–336.

Ziegler, A., H. Fabritius, and M. Hagedorn. 2005. Microscopical and functional aspects of calcium-transport and deposition in terrestrial isopods. *Micron* **36:** 137–153.